Nuclear Materials and Energy 000 (2017) 1–4

Contents lists available at ScienceDirect

Nuclear Materials and Energy

journal homepage: www.elsevier.com/locate/nme

Recent advances towards a lithium vapor box divertor

R.J. Goldston*, A. Hakim, G.W. Hammett, M.A. Jaworski, J. Schwartz

Princeton Plasma Physics Laboratory, Princeton, NJ 08543, USA

ARTICLE INFO

Article history:
Received 13 July 2016
Revised 29 November 2016
Accepted 9 March 2017
Available online xxx

ABSTRACT

Fusion power plants are likely to require near complete detachment of the divertor plasma from the divertor target plates, in order to have both acceptable heat flux at the target to avoid prompt damage and also acceptable plasma temperature at the target surface, to minimize long-term erosion. However hydrogenic and impurity puffing experiments show that detached operation leads easily to x-point MARFEs, impure plasmas, degradation in confinement, and lower helium pressure at the exhaust. The concept of the Lithium Vapor Box Divertor is to use local evaporation and strong differential pumping through condensation to localize low-Z gas-phase material that absorbs the plasma heat flux and so achieve detachment while avoiding these difficulties. The vapor localization has been confirmed using preliminary Navier–Stokes calculations. We use ADAS calculations of ε_{cool}, the plasma energy lost per injected lithium atom, to estimate the lithium vapor pressure, and so temperature, required for detachment, taking into account power balance. We also develop a simple model of detachment to evaluate the required upstream density, based on further taking into account dynamic pressure balance. A remarkable general result is found, not just for lithium-vapor-induced detachment, that the upstream density divided by the Greenwald-limit density scales as $n_{up}/n_{GW} \propto (P^{5/8}/B^{3/8})\, T_{det}{}^{1/2}/(\varepsilon_{cool} + \gamma T_{det})$, *with no explicit size scaling.* T_{det} is the temperature just before strong pressure loss, assumed to be ~ ½ of the ionization potential of the dominant recycling species, and γ is the sheath heat transmission factor.

1. The challenge

The heat flux and target electron temperature in a fusion power plant are likely to be higher than acceptable in standard "attached," or even "partially attached" divertor operation. However hydrogenic and impurity puffing experiments show that detached operation leads easily to x-point MARFEs, impure plasmas, degradation in confinement, and lower helium pressure at the exhaust. In the absence of a validated understanding of detachment, or scaling results as a function of heating power, it is not even clear whether detached solutions exist below the Greenwald limit at the very much higher parallel heat fluxes anticipated in a future fusion power system.

2. The lithium vapor box divertor

The concept behind the Lithium Vapor Box Divertor [1] is to control the location and density of low-Z vapor-phase material that absorbs the plasma heat flux, leading to plasma detachment. It uses local evaporation and strong differential pumping through condensation, as illustrated in Fig. 1, rather than allowing this to occur "naturally" through recycling of fuel gas and injected impurities. The configuration contains lithium vapor with margin in areal density along the divertor plasma to extinguish the maximum expected heat flux. Its bottom can be wetted with a layer of lithium to handle the highest transient heat fluxes. The upper boxes are much cooler than the bottom box, so lithium is redeposited there, greatly limiting the lithium efflux to the plasma in both steady-state and transient conditions. The required flow and inventory of lithium is modest, so can be circulated from the regions of net deposition to those of net evaporation via thin layers of capillary porous material along the surfaces, while some of the recirculating flow is extracted for purification.

This configuration should:

- Avoid instability to x-point MARFE formation, since as the detachment front moves towards the vapor-box entrance the lithium vapor density falls precipitously.
- Provide control over heat extraction from the plasma as a function of position along the divertor leg.
- Provide an efficient pump for impurities. The temperature in the top boxes can be set to pump hydrogenics, possibly He.

* Corresponding author.
E-mail address: goldston@pppl.gov (R.J. Goldston).

http://dx.doi.org/10.1016/j.nme.2017.03.020

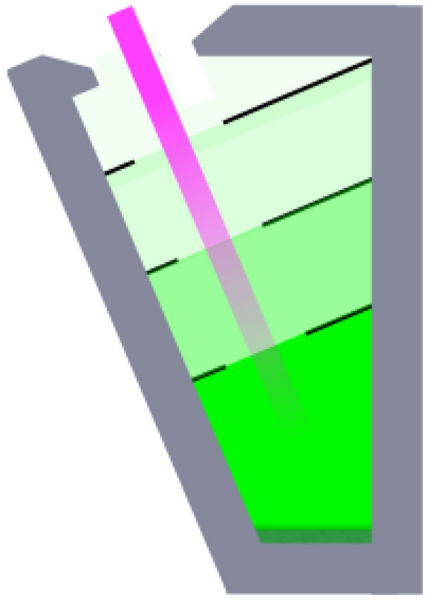

Fig. 1. Poloidal cross-section of lithium vapor box divertor.

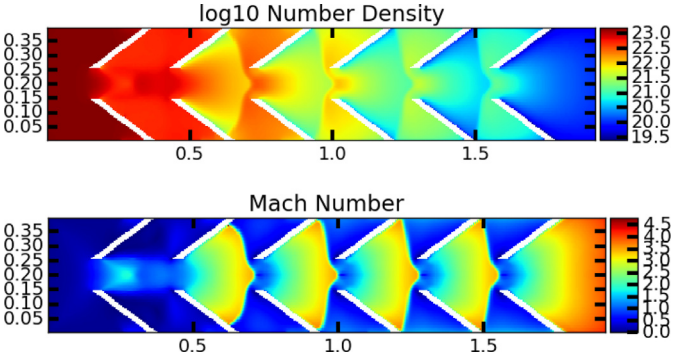

Fig. 2. Navier–Stokes calculation of number density and Mach number. White apertures are assumed reflecting.

- Be robust to changes in operating point. May tolerate ELMs, obviating the need for complex ELM-control coils that may not be practicable in a fusion reactor.

In recent work we have used inviscid Navier–Stokes calculations to confirm the estimates in [1] of the strong differential pumping capabilities of this system. These calculations, optimized for resolving shocks [2], model the evaporating and condensing surfaces using phantom boundary cells of Maxwellian vapor at the local wall temperature and equilibrium density. These cells absorb incoming vapor and emit vapor consistent with the equilibrium pressure. We have found, however, that reflecting surfaces must be included to induce standing shocks slowing the flow. The approximate condition for reflection is

$$n_{eq}(T_R)\sqrt{T_R} > n_{vap}\sqrt{T_{vap}} \tag{1}$$

where the subscript "*eq*" indicates the equilibrium lithium vapor pressure as a function of temperature, "*R*" indicates the reflecting surface, and "*vap*" indicates vapor quantities. Under these conditions, which should be straightforward to obtain because n_{vap} is always less than $n_{eq}(T_{vap})$, lithium will not be deposited on the reflector surface, and the normal flow to the surface will be halted. Fig. 2 shows the falling lithium density in a model Navier–Stokes calculation with reflecting surfaces.

3. Power balance

It is interesting to estimate the lithium vapor density required to extract a given amount of energy from the electron fluid in the plasma. Some of this energy is committed to ionization of the lithium, and some is lost through line and continuum radiation. (Some of the ionization energy will be returned to the electron fluid downstream, on recombination.) In our collisional-radiative model, as opposed to a pure coronal model, we used ADAS data to take into account nonlinear density effects including multi-step ionization, three-body recombination and collisional de-excitation. In order to approximate the realistic case where lithium has a finite residence time, we introduce neutral lithium as a source term in a charge-state model that includes a finite depletion time constant, τ_z, equal for all charge states. This model calculates the ionization and recombination rates into and out of each charge state, and includes both the neutral source term and the depletion of all charge states to determine the charge-state distribution. This allows calculation of the local cooling power density, whose units are W/m^3. Dividing this result by the particle source term (#/s m^3) provides a cooling energy per particle, ε_{cool}, as a function of T_e, n_e, and τ_z, as shown in Fig. 3. Because of the role of 3-body interactions, ε_{cool} depends on n_e and τ_z independently, not only in the combination $n_e\tau_z$. Considering the likely range of flow speeds of the lithium, and distance along *B*, we generally expect 10 μsec $< \tau_z <$ 1 msec. The longer times are associated with the higher temperatures.

These figures suggest cooling of order a few 100 eV per particle, mostly in the form of radiation, when the electron temperature is above about 30 eV, and about 10 eV per particle, mostly in the form of ionization, at significantly lower temperatures. However, based on a two-point model even with very high radiated power, an outer mid-plane SOL temperature of at least 200 eV should be expected in ITER, and of order 300 eV in a fusion power system. In this situation, the solution to the Spitzer conductivity equation with constant radiated power loss per unit length has more than 95% of the radiated power in the region with Te > 30 eV

If we assume that lithium vapor enters the divertor plasma from both sides at the Langmuir flow rate, $n\bar{v}/4$, and exits through the apertures shown in Fig. 1 with choked sonic flow, we can calculate both electron cooling and vapor efflux as functions of vapor temperature in the bottom-most box.

$$\frac{P_{dis}}{R\ell_{p,box}\varepsilon_{cool,eV}} = 4\pi e n_{eq}(T_{vap})\sqrt{T_{vap}/(2\pi m)} = \frac{\dot{M}}{5.62\cdot 10^{-8}Rd} \tag{2}$$

where P_{dis} is the power dissipated in a vapor box, $\ell_{p,\,box}$ is the poloidal extent of the box, $\dot{M}$ is the exit mass flow rate, and *d* is the exit aperture width. The first equality follows from assuming energy loss of $e\varepsilon_{cool,\,eV}$ Joules for each lithium atom entering the two sides of the divertor sheet of area $2\pi Rl_p$ at the Langmuir flux rate. The second equality follows from assuming choked flow efflux from an aperture of length $2\pi R$ and width *d*. This result is illustrated in Fig. 4. If we consider a fusion power plant with Q = 25 and P_{fus} = 2.5 GW, the total plasma heating power is 600 MW. If, like for ITER, we assume that there is significant core radiation such that 1/3 of this power travels down the outer divertor leg, this gives a required dissipated power of 200 MW. Eq. (2) and Fig. 4 then, with R = 6 m, $\ell_{p,\,box}$ = 0.5 m and ε_{cool} = 250 eV, give about 580 °C. The mass efflux through a 20 cm aperture would be 18 g/s. Based on the results shown in Fig. 2, this could easily be differentially pumped to much less than 1 g/s. NSTX has successfully operated [3] with continuous injection of 0.22 g/sec of lithium, indeed with improved plasma performance and neutron production, so an injection rate of 1 g/sec should be trivial for a fusion power plant. The vapor will not penetrate through the outer scrape-off layer and the resulting cooling rate, at 250 eV per particle, is only

Please cite this article as: R.J. Goldston et al., Recent advances towards a lithium vapor box divertor, Nuclear Materials and Energy (2017), http://dx.doi.org/10.1016/j.nme.2017.03.020

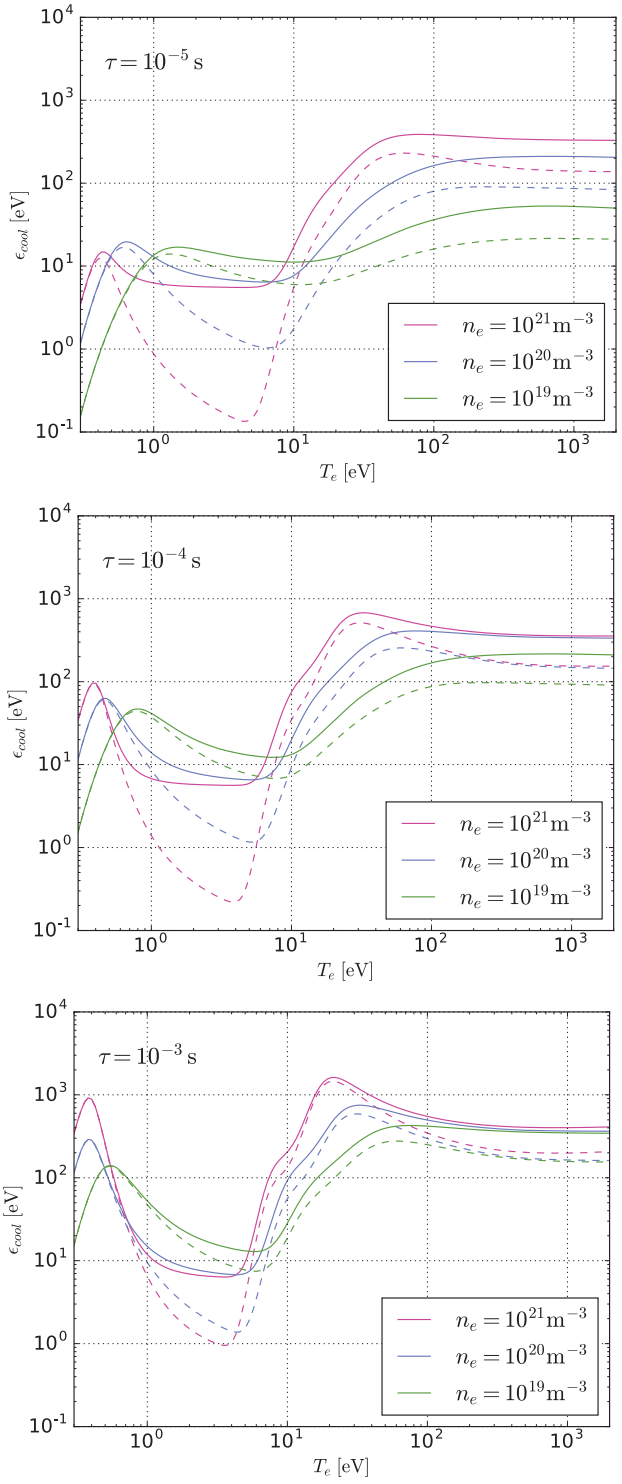

Fig. 3. ε_{cool} as a function of electron temperature and density. Dashed lines are radiation-only. (a): $\tau_z = 10$ μsec. (b): $\tau_z = 100$ μsec. (c): $\tau_z = 1$ msec.

3.4 MW. It will be necessary, however, for the chamber walls to be operated at high enough temperature that lithium does not condense and accumulate on them over time, and so can be removed in a lower-temperature region. The typical planned operating point of tokamak first walls, ≥ 500 °C, should be more than adequate.

From the point of view of power balance, it appears that a relatively compact lithium vapor box could be used to detach the plasma from a full power tokamak fusion reactor, with modest impact on the size of the system or on plasma performance.

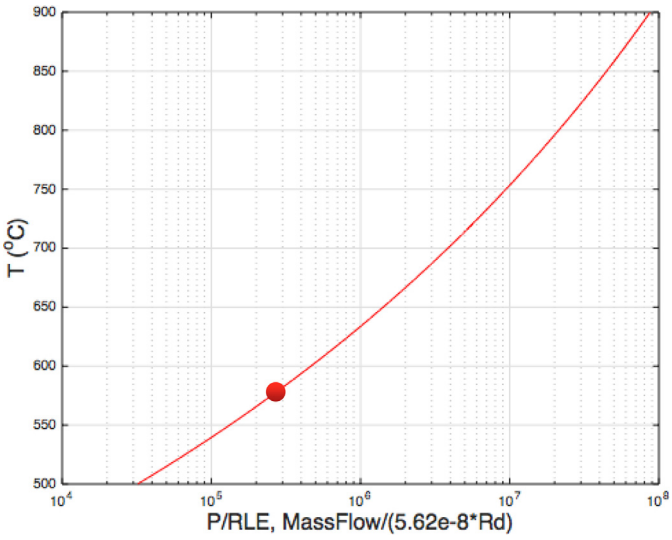

Fig. 4. Vapor temperature as a function of required dissipation power, with resulting mass efflux.

4. Upstream density for detachment

We now examine the issue of force (or pressure) balance, which determines the upstream density required for detachment both with a lithium vapor box divertor and more generally. The physics of detachment is not fully understood, and even empirical scaling studies are not in hand to project the crucial dependence of the required upstream n/n_{GW} on, inter alia, divertor power, machine size, and toroidal and poloidal field strengths for simple hydrogenic gas puffing (but see A.W. Leonard et al., this issue, for a good start). Here we resort to the tactic of assuming, based on observation, that detachment takes place soon after the target temperature drops to $T_{det} \sim 1/2$ of the dominant species ionization potential, while still maintaining dynamic pressure balance to this point. We use the standard 2-point model, extended [4] to take into account ε_{cool}, to find the upstream density needed to reach T_{det}.

For power balance we require,

$$\dot{N}e(\varepsilon_{cool,eV} + \gamma T_{det,eV}) = P_{div} \tag{3}$$

where $\dot{N}$ represents the total recycling source of hydrogenics or lithium and P_{div} is the power flowing into the divertor leg. For particle balance (assuming that the recycling source dominates, and M = 1 at the target) we require

$$\dot{N} = n_{det}(2eT_{det,eV}/m_i)^{1/2} 2\pi R_{OMP} \lambda_{\Gamma,OMP} (B_p/B)_{OMP} \tag{4}$$

where λ_Γ is the particle flux width mapped to the outer mid-plane and n_{det} is the density at the target when $T = T_{det}$. Substituting $\dot{N}$ from Eq. (4) into Eq. (3), and solving for n_{det}, we have

$$n_{det} = \frac{P_{div}}{e(\varepsilon_{cool,eV} + \gamma T_{det,eV})} \left(\frac{m_i}{2eT_{det,eV}}\right)^{1/2} \times \left[2\pi R_{OMP} \lambda_{\Gamma,OMP} (B_p/B)_{OMP}\right]^{-1} \tag{5}$$

Next we use the Heuristic Drift (HD) model [5] for the heat flux width, with a factor of 0.8 decrease to account for the best fit to the dataset reported by Eich [6], and a factor of 2 increase for diffusive spreading (S) below the X-point, $\lambda_{int} \sim 2\lambda_q$, based on the same dataset. We then use Spitzer conductivity to determine the

Please cite this article as: R.J. Goldston et al., Recent advances towards a lithium vapor box divertor, Nuclear Materials and Energy (2017), http://dx.doi.org/10.1016/j.nme.2017.03.020

Table 1
Projected upstream densities for nominal DIII-D, JET, ITER and Demo parameters. Demo is presumed to be geometrically similar to ITER, but operating at 7T and producing 2.5 GW(th) at Q = 25. Hydrogenic cooling on the left, Li cooling on the right.

	DIII-D (DD)	JET (DD)	ITER (DT)	Demo (DT)	DIII-D (Li)	JET (Li)	ITER (Li)	Demo (Li)
R	1.65	3	6.2	6.2	1.65	3	6.2	6.2
a	0.6	0.85	2	2	0.6	0.85	2	2
B	1.6	2.5	5	7	1.6	2.5	5	7
I_p	9E+05	2.5E+06	1.5E+07	2.1E+07	9E+05	2.5E+06	1.5E+07	2.1E+07
$<B_p>$	0.206	0.404	1.030	1.442	0.206	0.404	1.030	1.442
P_{div}	1.7E+06	8E+06	5E+07	2E+08	1.7E+06	8E+06	5.0E+07	2E+08
L_{det}	1.56E+01	2.83E+01	5.84E+01	5.84E+01	1.56E+01	2.83E+01	5.84E+01	5.84E+01
A_i	2.00E+00	2.00E+00	2.50E+00	2.50E+00	6.90E+00	6.90E+00	6.90E+00	6.90E+00
$T_{det,\,eV}$	6.80E+00	6.80E+00	6.80E+00	6.80E+00	2.70E+00	2.70E+00	2.70E+00	2.70E+00
$\lambda_{int}/\lambda_{\Gamma}$	5.00E-01	5.00E-01	5.00E-01	5.00E-01	5.00E-01	5.00E-01	5.00E-01	5.00E-01
$\varepsilon_{cool,eV}$	3.00E+01	3.00E+01	3.00E+01	3.00E+01	2.50E+02	2.50E+02	2.50E+02	2.50E+02
n_{up}	3.22E+19	7.84E+19	1.75E+20	5.13E+20	7.66E+18	1.87E+19	3.99E+19	1.17E+20
n_{up}/n_{GW}	4.04E-01	7.12E-01	1.47E+00	3.07E+00	9.63E-02	1.70E-01	3.35E-01	7.01E-01

upstream temperature, and assume dynamic pressure balance between up and down stream, giving

$$n_{up} = \left(\frac{2}{7}\kappa_{0e}\right)^{2/7} \frac{(2m_i)^{1/2}}{e^{3/2}} \left(\frac{\lambda_{int,OMP}}{\lambda_{\Gamma,OMP}}\right) \left(\frac{P_{div}(B/B_p)_{OMP}}{2\pi R_{OMP}\lambda_{int,OMP}}\right)^{5/7} \times \left(\frac{1}{L_{det}}\right)^{2/7} \frac{T_{det,eV}^{1/2}}{\left(\varepsilon_{cool,eV} + \gamma T_{det,eV}\right)} \quad (6)$$

where

$$\lambda_{int,OMP} = 1.6 \cdot 5671 \cdot P_{div}^{1/8} \frac{(1+\kappa^2)^{5/8} a^{17/8} B^{1/4}}{I_p^{9/8} R} \left(\frac{2\bar{A}}{\bar{Z}^2(1+\bar{Z})}\right)^{7/16} \times \left(\frac{Z_{eff}+4}{5}\right)^{1/8} \frac{R\langle B_p\rangle}{(R+a)B_{p,OMP}} \quad (7)$$

The scaling of n_{up}/n_{GW} at fixed shape and aspect ratio is then

$$\frac{n_{up}}{n_{GW}} \propto \frac{P_{div}^{5/8} B_t^{1/4}}{B_p^{5/8}} \frac{T_{det}^{1/2}}{\varepsilon_{cool} + \gamma T_{det}} \quad (8)$$

If the power scaling of Eq. (7) is neglected, then Eq. (8) gives $n_{up} \propto {P_{div}}^{5/7}/R$ at fixed B_t, B_p and impurity concentration. This scaling was compared with results from a related 1-D analysis [7] for a test case with 3% nitrogen density and $T_{det} = 6.8$ eV, where momentum loss is negligible [8]. The scaling coefficient with R at nearly fixed P_{div} (and so nearly fixed $T_{up} = 121$ eV) came out to be −1.0. The scaling coefficient with P_{div} at fixed R (with T_{up} varying from 87 to 175 eV) came out to be +0.63. (See reference [9] for an analysis that explicitly includes the variation of cooling efficiency with temperature.) The scaling with B in Eq. (8) follows from the definition of the Greenwald limit and the choice for the scaling of λ, so is explicitly identical with the 1-D analysis under identical assumptions about λ. As shown in Table 1, the absolute values resulting from Eq. (6) are reasonable for present experiments, and the projection for the lithium vapor box is promising, although in the case of Demo additional radiating species will likely be required, but considerable margin is available in Demo above the H-mode power threshold.

In general, the scaling with power and magnetic fields in Eq. (8) should be sufficient, for a given impurity mix, to allow scaling of the upstream density needed for detachment from present devices to future ones. The absence of any explicit size scaling may have important general implications, since the upstream SOL density most likely cannot exceed the pedestal density, which is observed to be constrained by n_{GW}. Furthermore, there is evidence that the upstream SOL density itself may be constrained by MHD stability not to exceed $\sim n_{GW}/3$ [10]. Detailed measurements on AUG [11] show $\eta_e \sim 1.4$ in the SOL as well as in the pedestal gradient region. If the outer midplane SOL density approaches the Greenwald limit, and the outer midplane SOL temperature is only a factor ~ 2 – 3 above present experiments, a limit to η_e would significantly restrict the achievable pedestal top temperature. Perhaps most importantly, this result also suggests that moving to a larger size fusion power plant, even at fixed separatrix loss power, does not mitigate the problem of needing a high upstream density relative to the Greenwald limit for detachment.

As an aside, we note that the observation of constant η_e on AUG suggests a physical mechanism, such as ETG modes, that couples the SOL electron thermal heat flux width, through the T_e profile, to the density profile. Such coupling is an essential feature of the HD model.

5. Future plans

We plan to model vapor transport using the Direct Simulation Monte–Carlo package available in OpenFOAM, which allows flow studies with arbitrary collisionality. We will examine a reactor implementation, an implementation in NSTX-U, and a bench simulation experiment. In parallel with the simulation experiment, measurements on NSTX-U should permit studies of lithium ε_{cool} and its dependencies.

Acknowledgments

This work supported by DOE Contract No. DE-AC02-09CH11466.

References

[1] R.J. Goldston, R. Myers, J. Schwartz, The lithium vapor Box divertor, Phys. Scr. T167 (2016) 014017.
[2] J.O. Langseth, R.J. LeVeque, A wave propagation method for three-dimensional hyperbolic conservation laws, Journal of Computational Physics 165 (1) (2000) 126–166.
[3] D.K. Mansfield, Fusion Eng. Des. 85 (2010) 890–895.
[4] P.C. Stangeby, The Plasma Boundary of Magnetic Fusion Devices, Section 5.5, IOP Publishing, Bristol UK, 2000.
[5] R.J. Goldston, Heuristic drift-based model of the power scrape-off width in low-gas-puff H-mode Tokamaks, Nucl. Fusion 52 (2012) 013009.
[6] T. Eich, Scaling of the tokamak near scrape-off layer H-mode power width and implications for ITER, Nucl. Fusion 53 (2013) 093031.
[7] A. Kallenbach, et al., Analytical calculations for impurity seeded partially detached divertor conditions, Plasma Phys. Control. Fusion 58 (2016) 045013.
[8] A. Kallenbach, A. Scarabosio, M. Siccinio, private communication, July 2016
[9] R.J. Goldston, M.L. Reinke, J.A. Schwartz, A new scaling for divertor detachment, Plasma Phys. Control. Fusion 59 (2017) 055015.
[10] R.J. Goldston, Theoretical aspects and practical implications of the heuristic drift SOL model, J. Nucl. Mat. 463 (2015) 397.
[11] H.J. Sun, Study of near scrape-off layer (SOL) temperature and density gradient lengths with Thomson Scattering, Plasma Phys. Control. Fusion 57 (2015) 125011.

Please cite this article as: R.J. Goldston et al., Recent advances towards a lithium vapor box divertor, Nuclear Materials and Energy (2017), http://dx.doi.org/10.1016/j.nme.2017.03.020